Selected Paper

Strong Interaction between Carbonyl and Dioxolene Ligands Caused by Charge Distribution of Ruthenium–Dioxolene Frameworks of Mono- and Dicarbonylruthenium Complexes

Tohru Wada, Tetsuaki Fujihara, Mizuno Tomori,[1] Dai Ooyama,[1] and Koji Tanaka*

Institute for Molecular Science and CREST, Japan Science and Technology Agency (JST), Nishigo-Naka, Okazaki 444-8585

[1]Faculty of Education, Fukushima University and CREST, Japan Science and Technology Agency (JST), Kanayagawa, Fukushima 960-1296

Received August 25, 2003; E-mail: ktanaka@ims.ac.jp

Monocarbonylruthenium complexes with a semiquinone ligand, $([Ru(CO)(sq)(L)]^{n+}$ (sq = 3,5-di-*tert*-butyl-1,2-benzosemiquinone, $n = 1$ or 0, L = 2,2′:6′,2″-terpyridine ($[\mathbf{1}]^+$), 2,6-bis(*N*,*N*-dimethylaminomethyl)pyridine ($[\mathbf{2}]^+$), 2,6-di-2′-pyridylphenyl ($[\mathbf{3}]^0$), or 2-(2,2′-bipyridin-6-yl)phenolato ($[\mathbf{4}]^0$)), and dicarbonylruthenium complexes with two semiquinone ligands, $[Ru(CO_2)_2(sq)_2]$ ($[\mathbf{5}]^0$) and $[Ru(CO)_2(phsq)_2]$ (phsq = 9,10-phenanthrasemiquinone, $[\mathbf{6}]^0$), were synthesized and the structures of $[\mathbf{1}]^+$ and [**6**] were determined by X-ray crystal analysis. Monocarbonyl Ru(II)–dioxolene complexes displayed the ligand localized catecholato/semiquinone and semiquinone/quinone redox couples, and two sets of those redox couples were observed in the dicarbonyl Ru(II)–bis(dioxolene) complexes. Spectroelectrochemical study revealed that the Ru(II)–catecholato and Ru(II)–semiquinone complexes were stable in solutions, while the Ru(II)–quinone complexes underwent fragmentation in solutions. One-electron reduction of the monocarbonyl Ru(II)–semiquinone complexes caused a red shift of the ν(CO) bands in a range of 41 to 56 cm^{-1}, which was substantially larger than those of carbonyl Ru(II)–polypyridyl complexes. Two ν(CO) bands of dicarbonyl Ru(II)–bis(semiquinone) complexes also shifted to lower wavelength in a range of 53 to 99 cm^{-1} upon two electron reduction of the complexes. The unusually large red shift of ν(CO) bands upon reduction of carbonyl Ru(II)–dioxolene complexes compared with those of Ru(II)–polypyridyl complex is ascribed to a strong electronic interaction between carbonyl and dioxolene ligands.

There is great interest in metal complexes having non-innocent ligands such as dioxolenes, dithiolenes and benzoquinonediimines. Dioxolenes take three oxidation states (quinone, semiquinone, and catechol). Orbital energies of the central metal and the dioxolene ligand in ruthenium–dioxolene complexes are unusually close to each other. Dioxolene–metal complexes, therefore, are characterized by charge distribution due to delocalization of π-electrons over the central metal and the ligand.[1] Consequently, Ru(II)–semiquinone and Ru(III)–catecholato, and Ru(II)–quinone and Ru(III)–semiquinone are expressed by forms in resonance with each other (Scheme 1).[2] We have reported the electrochemical behavior of [Ru(X)(dioxolene)(terpy)]^n (X = Cl^-, CH_3COO^-,[3] H_2O,[4] and CO,[5] terpy = 2,2′:6′,2″-terpyridine). Those complexes showed dioxolene-based and metal-centered redox reactions. The redox potentials of those reactions were largely dependent on both the substituents on dioxolene and the ligands X. For example, a Ru–semiquinone complex [RuCl(sq)(terpy)] underwent one-electron reduction and oxidation at $E_{1/2} = -1.07$ and -0.23 V (Cp_2Fe^+/Cp_2Fe), respectively, to give the corresponding catecholato (cat) and quinone (q) complexes,[3] while the cat/sq and sq/cat redox couples of $[Ru(CO)(sq)(terpy)]^+$ were observed at $E_{1/2} = -0.72$ and $+0.33$ V, respectively.[5] Thus, replacement of Cl with CO gave pronounced influences on the dioxolene-based redox potentials across Ru(II). To evaluate the interaction between dioxolene and CO ligands, we prepared a series of monocarbonylruthenium complexes $[Ru(CO)(sq)(L)]^{n+}$ (L = terpy ($[\mathbf{1}]^+$), bdap (2,6-bis(*N*,*N*-dimethylaminomethyl)pyridine, ($[\mathbf{2}]^+$)), dpp (2,6-di-2′-pyridylphenyl, ($[\mathbf{3}]^0$)), bph (2-(2,2′-bipyridin-6-yl)phenolato, ($[\mathbf{4}]^0$)), and dicarbonylruthenium complexes $[Ru(CO)_2(sq)_2]$ ($[\mathbf{5}]^0$) and $[Ru(CO)_2(phsq)]$

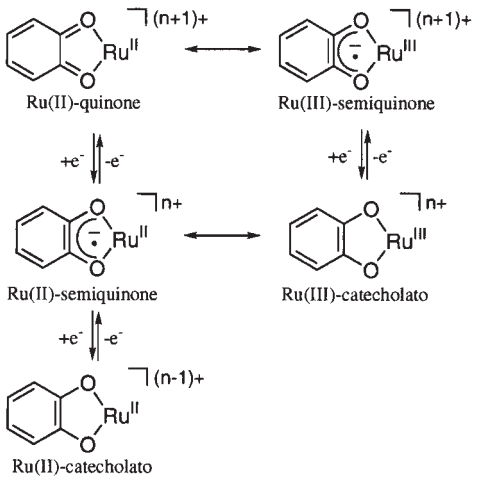

Scheme 1.

Published on the web April 2, 2004; DOI 10.1246/bcsj.77.741

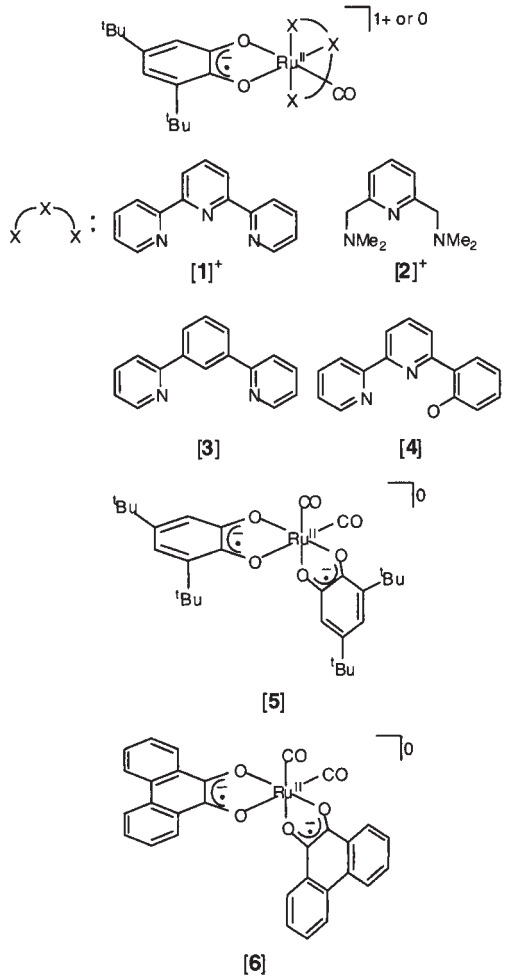

Chart 1.

(phsq = 9,10-phenanthrasemiquinone, ([**6**]^0)) (Chart 1). Reported here are the characterization and the redox properties of these complexes based on X-ray crystal analysis, EPR spectroscopy, electrochemistry, and spectroelectrochemistry.

Results and Discussion

Structure and Electronic State. The molecular structure of the complex cation of [**1**](ClO$_4$)·2(C$_7$H$_8$) was determined by X-ray analysis (Fig. 1). The details of data collection, refinement for the complex and selected bond lengths and angles are listed in Tables 1 and 2, respectively. The ruthenium atom adopts a slightly distorted octahedral configuration with two oxygen atoms of dioxolene, three nitrogen atoms of terpyridine and carbonyl carbon. The angles of O(1)–Ru–O(2) and N(1)–Ru–N(2) are 79.41(10)° and 79.9(1)°, respectively, and those of O(1)–Ru–C(30) and O(2)–Ru–N(2) are 173.4(1)° and 169.5(1)°, respectively. Although two structural isomers with respect to the orientation of *tert*-butyl groups on the dioxolene ligand would be produced in the reaction mixture, one isomer bearing two *tert*-butyl groups linked to C3 and C5 carbons of the dioxolene ligand was selectively crystallized out of the solution under the experimental conditions. The C–O bond length of carbonyl ligand is 1.102(5) Å. The C–O bond distances of dioxolene of 1.299(4) (C1–O1) and 1.293(4) Å (C2–O2) are close to those of sq (1.327(15) and 1.289(14) Å) in

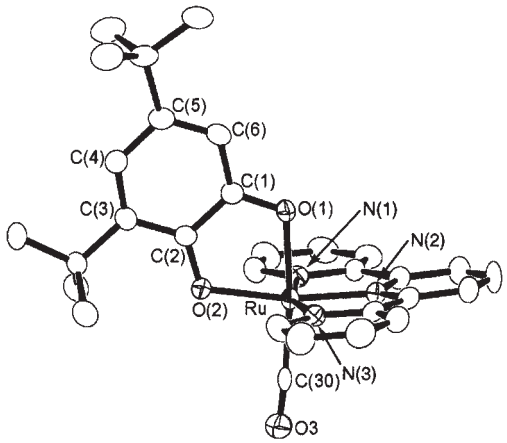

Fig. 1. ORTEP view of crystal structure of [**1**]$^+$. Thermal ellipsoids are drawn at the 50% probability lebel. Hydrogen atoms are omitted for clarity.

Table 1. Crystal Data and Structure Refinement for [**1**](ClO$_4$)·2(C$_7$H$_8$) and [**6**]

	[**1**](ClO$_4$)·2(C$_7$H$_8$)	[**6**]
Formula	$C_{30}H_{31}N_3O_3PF_6Ru\cdot 2(C_7H_8)$	$C_{30}H_{16}O_6Ru$
Formula weight	773.34	549.16
Temperature/K	173	173
Cryastal system	tricrinic	tricrinic
Space group	$P\bar{1}$ (No. 2)	$P\bar{1}$ (No. 2)
a/Å	12.105(5)	7.760(5)
b/Å	12.580(4)	8.608(6)
c/Å	13.919(5)	17.15(1)
α/deg	78.61(1)	97.55(1)
β/deg	83.608(9)	89.864(6)
γ/deg	86.53(1)	98.72(1)
V/Å^3	2063(1)	1122(1)
Z	2	2
d_{calcd}/g cm^{-3}	1.37	1.62
No. of unique reflns	9066	4894
No. of obsed reflns	7185, $I > 3\sigma(I)$	4331, $I > 2\sigma(I)$
$R1$ [$I > 2\sigma(I)$][a)]	0.052	0.049
$wR2$ [$I > 2\sigma(I)$][a)]	0.140[b)]	0.105[c)]

a) $R1 = \Sigma||F_o| - |F_c||/\Sigma|F_o|$, $wR2 = \{[\Sigma w(F_o^2 - F_c^2)^2]/\Sigma[w(F_o^2)^2]\}^{1/2}$, $w = \{\sigma^2(F_o)^2 + [p(\max(F_o^2, 0) + 2F_c^2)/3]^2\}^{-1}$. b) $p = 0.08$. c) $p = 0.03$.

[Ru^{II}(bpy)$_2$(sq)](ClO$_4$),[1o] and are clearly shorter than catecholato ligands.[3] Thus, the dioxolene ligand of [**1**]$^+$ is bonded to Ru as the semiquinone form. The electronic structure of the complex, therefore, was represented as [Ru^{II}(CO)(sq)(terpy)]$^+$. Indeed, [**1**](PF$_6$) displayed a sharp EPR signal at $g = 2.00$ with peak to peak separation of 5.39 G resulting from the semiquinone radical in CH$_2$Cl$_2$. The monocarbonyl complexes of [**2**](PF$_6$), [**3**], and [**4**] having bdap, dpp, and bph ligands, respectively, also showed the EPR spectra similar to those of [**1**](PF$_6$). [**2**]$^+$, [**3**] and [**4**] were, therefore, concluded to have the Ru(II)–semiquinone framework similarly to [**1**]$^+$. We also prepared [**5**] and [**6**] as dicarbonylruthenium complexes with two dioxolenes. We could not obtain single crystals of [**5**], but brown crystals of [**6**] suitable for X-ray analysis were obtained by recrystallization of the complex from CH$_2$Cl$_2$. The

Table 2. Selected Bond Lengths and Angles of [**1**](ClO_4)·2(C_7H_8)

Bond	Length/Å	Bond	Length/Å
Ru–O(1)	2.075(3)	Ru–O(2)	2.057(3)
Ru–N(1)	2.073(3)	Ru–N(2)	1.972(3)
Ru–N(3)	2.084(3)	Ru–C(30)	1.884(4)
C(30)–O(3)	1.102(5)		
O(1)–C(1)	1.299(4)	O(2)–C(2)	1.293(4)
C(1)–C(2)	1.451(5)	C(2)–C(3)	1.437(5)
C(3)–C(4)	1.358(5)	C(4)–C(5)	1.435(6)
C(5)–C(6)	1.371(6)	C(6)–C(1)	1.416(5)
Bond	Angles/deg	Bond	Angles/deg
O(1)–Ru–O(2)	79.41(10)	O(1)–Ru–N(1)	89.2(1)
O(1)–Ru–N(2)	90.1(1)	O(1)–Ru(1)–N(3)	88.4(1)
O(1)–Ru–C(30)	173.4(1)	O(2)–Ru–N(1)	98.8(1)
O(2)–Ru–N(2)	169.5(1)	O(2)–Ru–N(3)	101.1(1)
O(2)–Ru–C(30)	94.0(1)	N(1)–Ru–N(2)	79.9(1)
N(1)–Ru–N(3)	159.2(1)	N(1)–Ru–C(30)	91.9(1)
N(2)–Ru–N(3)	79.4(1)	N(2)–Ru–C(30)	96.4(1)
N(3)–Ru–C(30)	92.8(1)		

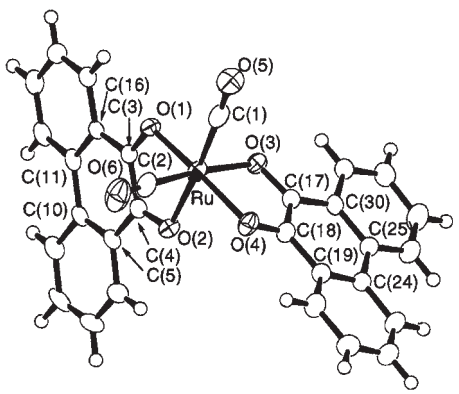

Fig. 2. ORTEP view of crystal structure of [**6**]. Thermal ellipsoids are drawn at the 50% probability level.

molecular structure of [**6**] determined by X-ray analysis is depicted in Fig. 2, and their selected bond lengths and angles are listed in Table 3. The ruthenium atom adopts a slightly distorted octahedral configuration like that of [**1**]. The carbonyl groups are located in a *cis* position with the C(1)–Ru–C(2) bond angle of 88.7(2)°. The bond distances of Ru–O(2) (2.092(2) Å) and Ru–O(3) (2.088(3) Å), which are *trans* to the Ru–CO bonds, are somewhat longer than those of Ru–O(1) (2.051(2) Å) and Ru–O(4) (2.055(3) Å), which are *cis* to the Ru–CO bonds. The O(2)–Ru–C(1) (174.5(1)°) and O(3)–Ru–C(2) (174.1(1)°) bond angles are close to 180°, while the O(1)–Ru–O(4) (166.39(10)°) bond angle largely deviates from a straight line. The CO bond lengths of dioxolenes are 1.296(4) and 1.306(4) Å, which also indicate the Ru(II)–bis(semiquinone) structure. Two CO ligands are located at *cis* positions in an equatorial plane and both C–O bond lengths are 1.120(5) Å, which are somewhat longer than that of [**1**]$^+$. Pierpont et al. reported the synthesis of [$Ru(CO)_2$(3,6-dbsq)$_2$] (3,6-dbsq = 3,6-di-*tert*-butyl-1,2-benzosemiquinone) as an isomer of [**5**] with a Ru(II)–bis(semiquinone) moiety.[6] The analogous isomer [**5**] also must have the same Ru(II)–bis(semiquinone) structure because the positions of two *tert*-butyl groups hardly affect the electronic structure of the complex. The absence of any EPR signals of [**5**] and [**6**] in CH_2Cl_2 at 173 K is indication of the occurrence of anti-ferromagnetic interaction between two unpaired electrons on two semiquinone groups.

Table 3. Selected Bond Lengths and Angles of [**6**]

Bond	Length/Å	Bond	Length/Å
Ru(1)–O(1)	2.051(2)	Ru(1)–O(2)	2.092(2)
Ru(1)–O(3)	2.088(3)	Ru(1)–O(4)	2.055(3)
Ru(1)–C(1)	1.880(4)	Ru(1)–C(2)	1.866(5)
C(1)–O(5)	1.120(5)	C(2)–O(6)	1.120(5)
O(1)–C(3)	1.296(4)	O(2)–C(4)	1.296(4)
C(3)–C(4)	1.437(5)	C(4)–C(5)	1.452(5)
C(5)–C(10)	1.411(5)	C(10)–C(11)	1.475(5)
C(11)–C(16)	1.413(5)	C(16)–C(3)	1.436(5)
O(3)–C(17)	1.306(4)	O(4)–C(18)	1.296(4)
C(17)–C(18)	1.424(5)	C(18)–C(19)	1.436(5)
C(19)–C(24)	1.401(5)	C(24)–C(25)	1.479(5)
C(25)–C(30)	1.424(5)	C(30)–C(17)	1.443(5)
Bond	Angles/deg	Bond	Angles/deg
O(1)–Ru–O(2)	80.38(9)	O(1)–Ru–O(3)	90.2(1)
O(1)–Ru–O(4)	166.39(10)	O(1)–Ru–C(1)	94.1(1)
O(1)–Ru–C(2)	94.7(1)	O(2)–Ru–O(3)	85.5(1)
O(2)–Ru–O(4)	89.09(10)	O(2)–Ru–C(1)	174.5(1)
O(2)–Ru–C(2)	92.1(1)	O(3)–Ru–O(4)	80.3(1)
O(3)–Ru–C(1)	94.2(1)	O(3)–Ru–C(2)	174.1(1)
O(4)–Ru–C(1)	96.3(1)	O(4)–Ru–C(2)	94.3(1)
C(1)–Ru–C(2)	88.7(2)		

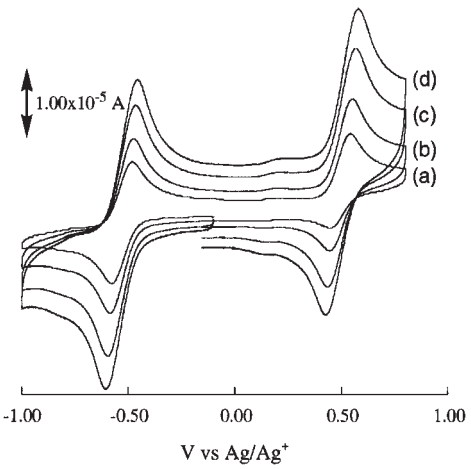

Fig. 3. The CV of [**1**](PF_6) in CH_2Cl_2 at various scanning rates; 50 (a), 100 (b), 200 (c), and 300 mV/s (d).

Electrochemistry. The CVs of the complexes were obtained in dichloromethane or 1,2-dichloroethane. The CV of [**1**](PF_6) showed two redox couples at $E_{1/2} = -0.58$ V and +0.49 V ($E_{1/2} = (E_{pa} + E_{pc})/2$) in a potential range from +1.0 to −1.0 V (vs Ag/Ag^+) in CH_2Cl_2 (Fig. 3). The peak separations of the redox couples increased from $\Delta E_p = 0.107$ V to 0.149 V on increasing the scan rates from 50 mV/s to 300 mV/s. These redox couples were, therefore, quasi-reversible. Based on the rest potential (−0.10 V) of the CH_2Cl_2 solution of [**1**]$^+$, the two redox reactions at $E_{1/2} = -0.58$ and +0.49 V were as-

signed to the ligand-based cat/sq and sq/q couples of $[\mathbf{1}]^+$ (Eq. 1), respectively. The assignment was consistent with the electronic absorption spectra of $[\mathbf{1}]^+$ under electrolysis conditions (Fig. 4). Electronic absorption spectra of $[\mathbf{1}]^+$ in dichloromethane showed strong bands at 645 nm and at 390 nm due to the metal to ligand charge transfer (MLCT) band of Ru(II)–sq and Ru(II)–terpy, respectively. Electrochemical reduction of $[\mathbf{1}]^+$ at -0.62 V in dichloromethane resulted in disappearance of the 645 nm band, while the 390 nm band shifted to 438 nm. Thus, [Ru(CO)(cat)(terpy)] formed by one-electron reduction of the sq ligand of $[\mathbf{1}]^+$ lost the MLCT band of the Ru(II)–sq framework at 645 nm and showed the red-shift of the MLCT band of the Ru(II)–terpy one from 390 nm to 438 nm due to an increase of d-orbital energy. Reoxidation of [Ru(CO)(cat)(terpy)] at 0.00 V fully recovered the 645 nm and 390 nm MLCT bands of $[\mathbf{1}]^+$ within ca. 30 min. On the other hand, one-electron oxidation of the sq ligand of $[\mathbf{1}]^+$ under the controlled potential electrolysis conditions at $+0.80$ V brought about gradual fragmentation of the complex probably due to lability of a Ru(II)–q framework.

$$[\mathrm{Ru(CO)(cat)(terpy)}]^0 \underset{+e^-,\ -0.58\ \mathrm{V}}{\overset{-e^-}{\rightleftharpoons}} [\mathrm{Ru(CO)(sq)(terpy)}]^+ \underset{+e^-,\ +0.49\ \mathrm{V}}{\overset{-e^-}{\rightleftharpoons}} [\mathrm{Ru(CO)(q)(terpy)}]^{2+} \quad (1)$$

The redox potentials of the present complexes are summarized in Table 4. The CV of $[\mathbf{2}](PF_6)$ also displayed two quasi-reversible redox couples of the cat/sq and sq/q couples at $E_{1/2} = -0.62$ and $+0.45$ V, respectively, in CH_2Cl_2. The redox potentials of the $[\mathbf{2}]^0/[\mathbf{2}]^+$ and $[\mathbf{2}]^+/[\mathbf{2}]^{2+}$ couples cathodically shifted by 40 mV based on those of the $[\mathbf{1}]^0/[\mathbf{1}]^+$ and $[\mathbf{1}]^+/[\mathbf{1}]^{2+}$ ones. This result reflects the difference in the electron donor ability between terpy and bdap ligands. Both dpp and bph of [**3**] and [**4**] are negatively charged terdentate ligands in contrast to neutral terpy and bdap ligands of $[\mathbf{1}]^+$ and $[\mathbf{2}]^+$. The redox potentials of [**3**] and [**4**] were observed at potentials more negative than those of $[\mathbf{1}]^+$ and $[\mathbf{2}]^+$.

The CV of a dicarbonyl complex [**5**] showed three quasi-reversible redox couples at $E_{1/2} = -0.83$, -0.44, and $+0.64$ V and one irreversible redox wave at $E_p = +0.95$ V (Fig. 5). The redox potentials at $E_{1/2} = -0.83$, -0.44, and $+0.64$ V were associated with the $[Ru(CO)_2(cat)_2]^{2-}/[Ru(CO)_2(sq)(cat)]^-$, $[Ru(CO)_2(sq)(cat)]^-/[Ru(CO)_2(sq)_2]^0$, and $[Ru(CO)_2(sq)_2]^0/[Ru(CO)_2(q)(sq)]^+$ couples, respectively. The remaining irreversible anodic peak at $E_p = +0.95$ V apparently results from the oxidative degradation of the resultant $[Ru(CO)_2(q)(sq)]^+$, because a Ru–CO bond cleavage was confirmed in the IR spectra of $[Ru(CO)_2(q)_2]^{2+}$ produced under the electrolysis at $+0.95$ V in dichloroethane. One-electrone reduction of [**5**] at -0.65 V caused the decrease of MLCT band based on the

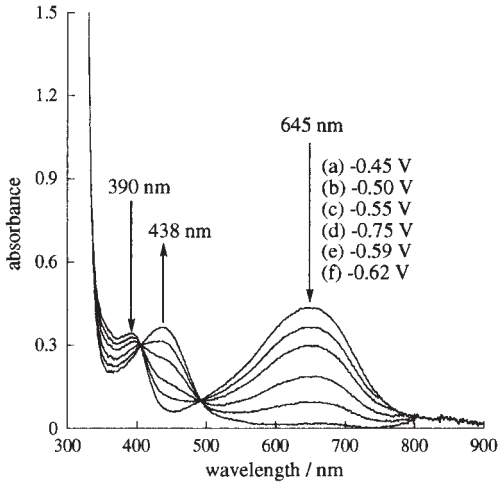

Fig. 4. UV–vis–NIR spectra of $[\mathbf{1}](PF_6)$ in CH_2Cl_2 under electrolysis conditions.

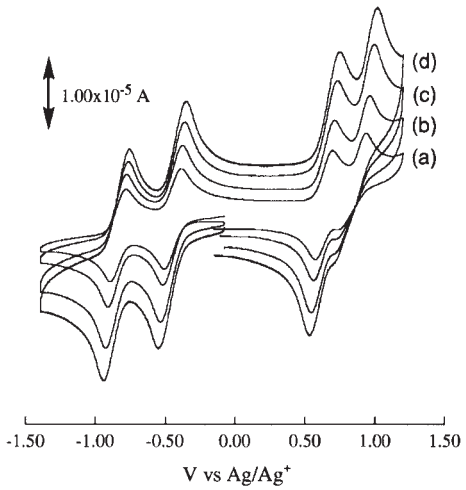

Fig. 5. The CV of [**5**] in CH_2Cl_2 at various scanning rates; 50 (a), 100 (b), 200 (c), and 300 mV/s (d).

Table 4. Redox Potentials and IR Data of the Mono and Dicarbonylruthenium Complexes

Complexes	Potentials/V vs Ag/Ag^+				ν(CO)/cm^{-1}							
	cat/sq		sq/q		cat state		MV state[c]		sq state		$\Delta\nu$(CO)	
$[\mathbf{1}](PF_6)$[a]	-0.58		$+0.49$		1927				1978		-51[d]	
$[\mathbf{2}](PF_6)$[a]	-0.62		$+0.45$		1905				1946		-41[d]	
$[\mathbf{3}]$[a]	-1.05		-0.07		1868				1923		-55[d]	
$[\mathbf{4}]$[a]	-0.76		$+0.19$		1881				1937		-56[d]	
$[\mathbf{5}]$[b]	-0.83	-0.44	$+0.64$	$+0.95$	1897	1990	1938	2013	1996	2054	-99[e]	-64[e]
$[\mathbf{6}]$[b]	-0.54	-0.28	$+0.66$	$+0.85$	1908	2002	1946	2026	1996	2055	-88[e]	-53[e]

CVs and IR spectra with electrolysis were determined in a) CH_2Cl_2 and b) 1,2-dichloroethane containing $^nBu_4N(ClO_4)$ or $^nBu_4N(PF_4)$ (0.1 M) as a supporting electrolyte. c) Ligand-based mixed valence state of $[Ru(CO)_2(sq)(cat)]^-$. d) Differences of ν(CO) bands between sq and cat states. e) Differences of ν(CO) bands between (sq)(sq) and (cat)(cat) states.

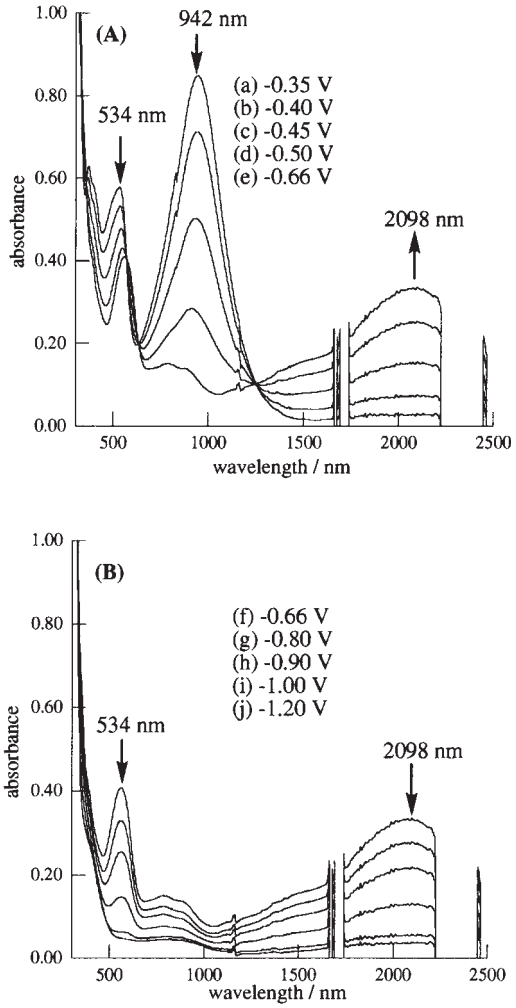

Fig. 6. UV–vis–NIR spectra of [**5**] with electrolysis at various potentials in 1,2-dichloroethane; reduction of [**5**] to $[\mathbf{5}]^{-}$ (A), and subsequent reduction of $[\mathbf{5}]^{-}$ to $[\mathbf{5}]^{2-}$ (B).

Ru(II)–sq framework at 942 nm and an appearance of a new band at 2089 nm (Fig. 6). A similar band of an analog of [**5**] has been assigned to the charge transfer band between sq and cat by Pierpont et al.[6] Indeed, the 2089 nm band of $[Ru(CO)_2(sq)(cat)]^{-}$ disappeared upon further one-electron reduction at −1.20 V because of the formation of $[Ru(CO)_2(cat)_2]^{2-}$. The dicarbonyl complex [**6**] also showed two successive reversible cat/sq redox couples at −0.54 and −0.28 V, and two sq/q redox couples at +0.66 and +0.85 V.

The ν(CO) Band Shifts of the Carbonyl Complexes. The ν(CO) bands of the present carbonyl complexes were observed in a range of 2100 to 1850 cm^{-1}. Those bands were sensitive to the oxidation states of dioxolene ligands as well as to the third ligand. For example, $[Ru(CO)Cl(bpy)_2]^{+}$ exhibited the ν(CO) at 1984 cm^{-1}.[7] Replacement of Cl^{-} of $[Ru(CO)Cl(bpy)_2]^{+}$ with CO as an electron withdrawing group caused a blue shift of the ν(CO) band from 1984 cm^{-1} to 2040 and 2085 cm^{-1}.[8] Table 4 summarizes the ν(CO) bands of the present ruthenium carbonyl complexes with semiquinone ligands. The ν(CO) bands of the complexes shifted to lower frequency in the order: $[\mathbf{1}]^{+}$ (1978 cm^{-1}) > $[\mathbf{2}]^{+}$ (1946 cm^{-1}) > [**4**] (1937 cm^{-1}) > [**3**] (1923 cm^{-1}), which apparently reflects the electron donor ability of the terdentate ligand to Ru. The red shift of the ν(CO) band of $[\mathbf{2}]^{+}$ compared with $[\mathbf{1}]^{+}$, therefore, results from the difference in the electron donor ability between dimethylamino groups of bdap and pyridyl groups of terpy. The appearance of the ν(CO) band of [**4**] and [**3**] at relatively lower wave number is ascribed to the Ru–C and Ru–O bond formed between the negatively charged terdentate dpp and bph ligands with Ru. Accordingly, the emergence of the ν(CO) band of the dicarbonyl complexes at higher wave length, [**5**] (1996, 2054 cm^{-1}) and [**6**] (1975, 2049 cm^{-1}) reflects the strong electron withdrawing ability of CO. As Ru–dioxolene complexes have a charge distribution of π-electrons over the central metal and the ligands, the ν(CO) bands of the complexes largely depend on oxidation states of the dioxolene ligands. The CV of $[\mathbf{1}](PF_6)$ showed the quasi-reversible cat/sq and sq/q redox couples at −0.58 V and +0.49 V, respectively. The electrolysis of $[\mathbf{1}](PF_6)$ at −0.80 V (vide infra $E_{1/2} = -0.58$ V) in CH_2Cl_2 smoothly proceeded and the ν(CO) band moved from 1978 cm^{-1} to 1927 cm^{-1} (Fig. 7). Reoxidation of the solution at 0.00 V fully recovered the IR spectrum of $[\mathbf{1}]^{+}$, indicating that $[\mathbf{1}]^{0}$ was stable in solutions. Thus, the red shift of the ν(CO) band of $[\mathbf{1}]^{+}$ caused by one-electron reduction (Eq. 2) is −51 cm^{-1}. It is worthy of note that semiquinone of $[\mathbf{1}]^{+}$ and quinoline of $[Ru(CO)(quinoline)(bpy)_2]^{+}$ are reduced at $E_{1/2} = -0.58$ V and $E_{1/2} = -1.21$ V, respectively, and the red shift of the ν(CO) band of $[Ru(CO)(quinoline)(bpy)_2](PF_6)_2$ caused by one-electron reduction was −35 cm^{-1} (from 2015 to 1980 cm^{-1}) (Eq. 3).[9]

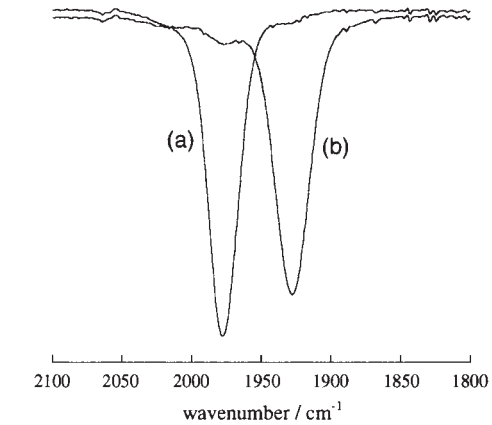

Fig. 7. IR spectra of $[\mathbf{1}]^{+}$ (a) and the one-electron reduced form (b) at −0.80 V (vs Ag/Ag^{+}) in CH_2Cl_2 containing $^{n}Bu_4N(ClO_4)$ (0.1 M).

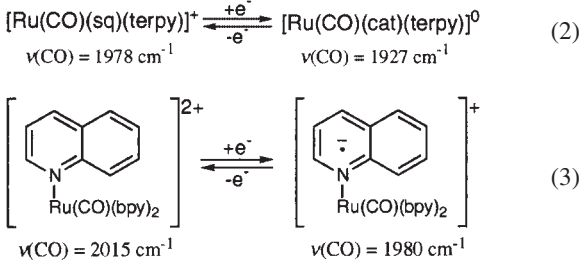

(2)

(3)

These results also are indication of the large charge distribution of Ru–dioxolene complexes compared with those of Ru–polypyridyl complexes. Similarly, $[\mathbf{2}](PF_6)$, [**3**], and [**4**] also showed the large red shift of the ν(CO) band upon one-electron reduction under the electrolysis conditions (Table 4), though

the degree of the shifts were not always proportional to the redox potentials of the sq/cat couple. On the other hand, one-electron oxidation of the complexes under the electrolysis in a potential range of +0.80 V resulted in gradual degradation of the complexes due to the lability of their Ru(II)–q frameworks, because the electronic absorption spectra of the complexes under the electrolysis conditions exhibited the formation of free quinone dissociated from the oxidized form of the complexes.

In contrast to mono-carbonyl complexes, $[\mathbf{1}]^+$, $[\mathbf{2}]^+$, [**3**], and [**4**], dicarbonyl complexes, [**5**] and [**6**] showed successive two quasi-reversible sq/cat redox couples (Fig. 5). Electrochemical reduction of [**5**] at −0.65 V shifted the ν(CO) bands at 1996 cm^{-1} and 2054 cm^{-1} to 1938 and 2013 cm^{-1} due to the formation of $[Ru(CO)_2(sq)(cat)]^-$ (Fig. 8(a)). Further one-electron reduction of $[Ru(CO)_2(sq)(cat)]^-$ at −1.20 V brought about the appearance of the ν(CO) bands at 1897 and 1990 cm^{-1} (Fig. 8(b)). Thus, the red shifts of the ν(CO) bands of [**5**] caused by one- and two-electron reduction were $\Delta\nu(CO) = -41$ and -58 cm^{-1}, and -64 and -99 cm^{-1}, respectively, (Eq. 4).

$$[Ru(CO)_2(sq)_2]^0 \underset{-e^-}{\overset{+e^-}{\rightleftharpoons}} [Ru(CO)_2(sq)(cat)]^{1-} \underset{-e^-}{\overset{+e^-}{\rightleftharpoons}} [Ru(CO)_2(cat)_2]^{2-} \quad (4)$$

ν(CO) = 1996, 2054 cm^{-1} ; ν(CO) = 1938, 2013 cm^{-1} ; ν(CO) = 1897, 1990 cm^{-1}

Similarly, the $\Delta\nu$(CO) values observed in one- and two-electron reduction of [**6**] were -29 and -50 cm^{-1}, and -53 and -88 cm^{-1}, respectively. We calculated the stretching force constants of the CO group to evaluate the interactions not only between CO and dioxolene but also between two CO ligands, since those interactions must be largely dependent on the oxidation state of dioxolene ligands. The CO stretching force constant (k) and the stretching–stretching interaction constant (k_i) of octahedral *cis*-dicarbonyl complexes are expressed by Eqs. 5 and 6,

$$\lambda_1 = \mu(k + k_i) \quad (5)$$

$$\lambda_2 = \mu(k - k_i), \quad (6)$$

where $\lambda = \{(2\pi c)^2/N_A\}\nu(CO)^2$ (N_A: Avogadro's constant), $\lambda_1 > \lambda_2$, and $\mu = N_A/m$ (m: reduced mass of CO group).[18] The k and k_i values of the dicarbonyl complexes are summarized in Table 5 together with the k values of the monocarbonyl complexes. Reduction of semiquinone to catecholato of $[\mathbf{1}]^+$, $[\mathbf{2}]^+$, [**3**], and [**4**] caused the changes of the k values in a range of $\Delta k = -64$ to -0.87 N cm^{-1}. Similarly, one-electron reduction of the dicarbonyl complexes, [**5**] and [**6**], resulted in the de-

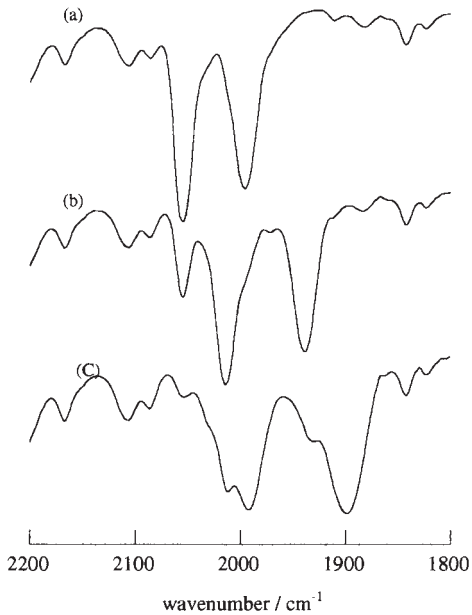

Fig. 8. IR spectra of $[\mathbf{5}]^0$ (a), the one-electron reduced form, $[\mathbf{5}]^-$ (b) at −0.65 V, and the two-electron reduced form, $[\mathbf{5}]^{2-}$ (c) at −1.20 V (vs Ag/Ag^+) in 1,2-dichloroethane containing $^nBu_4N(ClO_4)$ (0.1 M).

Table 5. Stretching Constant (k) and Stretching–Stretching Interaction Constant (k_i) of the Carbonyl Ligands of the Mono and Dicarbonylruthenium Complexes

	$k^{a)}$/N cm^{-1}				
Complexes	sq state, $k_{sq}{}^{a)}$		cat state, $k_{cat}{}^{a)}$	$\Delta k_1 = k_{cat} - k_{sq}$	
$[\mathbf{1}](PF_6)$	15.81		15.00	−0.81	
$[\mathbf{2}](PF_6)$	15.30		14.66	−0.64	
[**3**]	14.94		14.10	−0.84	
[**4**]	15.16		14.29	−0.87	
	cat state, $k_{sq}{}^{b)}$ (k_i)	MV state, $k_{MV}{}^{b)}$ (k_i)	sq state, $k_{sq}{}^{b)}$ (k_i)	$\Delta k_1 = k_{MV} - k_{sq}$	$\Delta k_2 = k_{cat} - k_{MV}$
[**5**]	16.56	15.77	15.26	−0.79	−0.51
	(0.47)	(0.60)	(0.73)		
[**6**]	16.57	15.93	15.44	−0.64	−0.49
	(0.48)	(0.64)	(0.74)		

a) Stretching constants of CO of the monocarbonyl complexes were calculated by the equation: $\nu(CO) = (k/m)^{1/2}/2\pi c$ (the reduced mass of CO group: $m = 1.139 \times 10^{-23}$ g, light velocity: $c = 2.9979 \times 10^{10}$ cm s^{-1}). b) Stretching constants and stretch–stretch interaction constant of CO of the monocarbonyl complexes were calculated by the equation: $\lambda_1 = \mu(k + k_i)$, $\lambda_2 = \mu(k - k_i)$ ($\lambda_1 > \lambda_2$, $\lambda = \{(2\pi c)^2/N_A\}\nu(CO)^2$, N_A = Avogadro's constant, c = light velocity, $\mu = N_A/m$).[18]

crease of the k values by 0.79 and 0.64 $N\,cm^{-1}$, respectively. The changes of the k values upon further one-electron reduction of $[\mathbf{5}]^-$ to $[\mathbf{5}]^{2-}$ and of $[\mathbf{6}]^-$ to $[\mathbf{6}]^{2-}$ were -0.51 and -0.49 $N\,cm^{-1}$, respectively. Thus, the reduction of $[Ru(CO)_2(sq)_2]^0$ to $[Ru(CO)_2(sq)(cat)]^-$ induced more serious change in the k values compared with the reduction of $[Ru(CO)_2(sq)(cat)]^-$ to $[Ru(CO)_2(cat)_2]^{2-}$. It is also worthy of note that the decrease of the k value of $[Ru(CO)(quinoline)(bpy)_2]^{2+}$ caused by quinoline-based one-electron reduction was 0.56 $N\,cm^{-1}$; this value is close to the Δk value induced by the reduction of $[Ru(CO)_2(sq)(cat)]^-$ to $[Ru(CO)_2(cat)_2]^{2-}$. The stretching–stretching interaction constant (k_i) increase in the order of $[Ru(CO)_2(sq)_2]^0 < [Ru(CO)_2(sq)(cat)]^- < [Ru(CO)_2(cat)_2]^{2-}$ is apparently consistent with the order of increasing the d-electron density of the Ru atom. Thus, the interaction between two carbonyl ligands is enhanced with the progress of the reduction of dioxolene ligands.

Despite the fact that semiquinone ligands are reduced to catecholato at potentials much more positive than the reduction of polypyridyl ones, the redox reaction of the former gives more serious electronic influence to the CO ligands compared with that of polypyridyl ones. Such a strong interaction between CO and dioxolene ligands across Ru(II) is explained by the effective mixing of 3d orbital (t_{2g}) of Ru(II) with LUMO of quinone (SOMO of semiquinone) compared with LUMO of polypyridyl ligands. In addition, the π^* orbital of CO located at a *trans*-position of dioxolene ligand also interacts with the same 3d orbital (t_{2g}) of Ru(II). The charge distribution in the Ru–dioxolene framework, therefore, largely enhances the interaction between SOMO of semiquinone and π^* orbital of carbonyl ligands in Ru–dioxolene complexes.

Experimental

Materials. $RuCl_3$ was purchased from Furuya Metal Co., Ltd., 3,5-di-*tert*-butylcatechol, 3,5-di-*tert*-butyl-1,2-benzoquinone, and 9,10-phenanthraquinone were from Tokyo Kasei Organic Chemicals; and 2,2′:6′,2″-terpyridine and $Ru_3(CO)_{12}$ were from Aldrich Chemical Co., Ltd. $[Ru(CO)_2Cl(NN'N)](OTf)$,[10] $[Ru(sq)_3]$,[11] 2-(2,2′-bipyrid-6-yl)phenol[12] were synthesized according to the literature. Solvents were distilled just prior to use.

Preparations of Complexes. [Ru(CO)(sq)(terpy)](PF$_6$), [1](PF$_6$): $Ru(CO)_2(sq)_2$, [**5**] (30 mg, 0.05 mmol), and 2,2′:6′,2″-terpyridine (12 mg, 0.05 mol) were refluxed in EtOH (15 mL) for 1 h under N_2. After the reaction mixture cooled to room temperature, NH_4PF_6 (20 mg) was added to the solution. The solvent was removed under reduced pressure, and the residue was dissolved in acetone followed by passing through an alumina column (2.5 × 10 cm). The second blue band was collected and evaporated to dryness. The crude product was dissolved in CH_3CN and addition of toluene to the solution afforded blue crystals, which were filtered off, washed with toluene, and dried under reduced pressure. Yield: 11 mg, 30%. IR (ν/cm^{-1}, KBr): 1977 (s, CO). UV–vis–NIR (λ_{max}/nm (ε/$M^{-1}\,cm^{-1}$), CH_2Cl_2): 644 (4390), 396 (3430), 324 (2580), 310 (2250), 284 (2540), 274 (2330). EPR (CH_2Cl_2 at 300 K): $g = 2.00$. ESI-MS (m/z, CH_2Cl_2): 583 ([**1**]$^+$). Anal. Found: C, 51.49; H, 4.62; N, 5.46%. Calcd for $C_{30}H_{31}N_3O_3PF_6Ru \cdot 0.5(C_7H_8)$: C, 51.63; H, 4.67; N, 5.47%.

[Ru(CO)(sq)(bdap)](PF$_6$), [2](PF$_6$): A methanolic solution of ^{t}BuOK (46 mg, 0.41 mmol) was added to a CH_2Cl_2 solution containing $[Ru(CO)_2Cl(bdap)](OTf)$ (100 mg, 0.19 mmol) and 3,5-di-*tert*-butylcatechol (42 mg, 0.19 mmol), and the mixture was stirred at room temperature for 8 h under N_2. The resultant yellow solution, probably containing [Ru(CO)(cat)(bdap)], was stirred again for another 3 h under the air, during which time the color of the solution turned to dark blue. Aqueous NH_4PF_6 was added to the solution. Evaporation of methanol under reduced pressure gave a dark blue solid, which was filtered off; crystallization from CH_2Cl_2/hexane afforded blue micro crystals. Yield: 81 mg, 62%. IR (ν/cm^{-1}, KBr): 1946 (s, CO). UV–vis–NIR (λ_{max}/nm (ε/$M^{-1}\,cm^{-1}$), CH_2Cl_2): 323 (9370), 687 (1000). EPR (CH_2Cl_2 at 300 K): $g = 2.00$. ESI-MS: m/z 543 ([**2**]$^+$). Anal. Found: C, 45.44; H, 5.77; N, 6.02%. Calcd for $C_{26}H_{39}N_3O_3RuPF_6$: C, 45.41; H, 5.72; N, 6.11%.

[Ru(CO)(sq)(dpp)], [3]: A 2-methoxyethanol solution (50 mL) containing $[Ru(sq)_3]$ (393 mg, 0.52 mmol) and 1,3-di-2′-pyridylbenzene (120 mg, 0.52 mmol) was refluxed for 8 h. The mixture was concentrated to about 1/5 under reduced pressure. An addition of water (30 mL) to the 2-methoxyethanol solution solution (10 mL) precipitated a purple solid, which was filtered off and dried in vacuo. To remove unreacted $[Ru(sq)_3]$, we suspended the crude product in hexane (10 mL) and filtered it. Such manipulation was repeated 5 times. Yield: 122 mg, 41%. IR (ν/cm^{-1}, KBr): 1918 (s, CO). UV–vis–NIR (λ_{max}/nm (ε/$M^{-1}\,cm^{-1}$), CH_2Cl_2): 363 (5500), 406 (5460), 766 (3410). EPR (CH_2Cl_2 at 300 K): $g = 2.00$. ESI-MS (m/z, CH_2Cl_2): 581 ([**3**]$^+$). Anal. Found: C, 60.01; H, 5.50; N, 4.29%. Calcd for $C_{31}H_{31}N_2O_3Ru \cdot 2H_2O$: C, 60.38; H, 5.72; N, 4.54%.

[Ru(CO)(sq)(dph)], [4]: An ethanol solution (15 mL) of $[Ru(CO)_2(sq)_2]$, [**5**] (48 mg, 0.08 mmol) and 2-(2,2′-bipyridin-6-yl)phenol (20 mg, 0.08 mol) was refluxed for 5 h under N_2. After the solvent was removed under reduced pressure, the residue was dissolved in CH_2Cl_2 followed by passing through a silica gel column (2.5 × 10 cm). The second green band was collected and evaporated to dryness. The residue was dissolved in CH_2Cl_2. An addition of Et_2O to the solution precipitated a green powder. The green compound was filtered off, washed with Et_2O, and dried under reduced pressure. Yield: 11 mg, 23%. IR (ν/cm^{-1}, KBr): 1938 (s, CO). UV–vis–NIR (λ_{max}/nm (ε/$M^{-1}\,cm^{-1}$), CH_2Cl_2): 691 (3420), 355 (7630), 305 (2410), 259 (2810). EPR (CH_2Cl_2 at 300 K): $g = 2.00$. ESI-MS (m/z, CH_2Cl_2): 597 ([**4**]$^+$). Anal. Found: C, 61.57; H, 5.56; N, 4.69%. Calcd for $C_{31}H_{31}N_2O_4Ru$: C, 62.40; H, 5.24; N, 4.69%.

[Ru(CO)$_2$(sq)$_2$], [5]: $[Ru(CO)_2(sq)_2]$ was synthesized according to the method of $[Ru(3,6\text{-}dbsq)_2(CO)_2]$ by using 3,5-di-*tert*-butylbenzoquinone instead of 3,6-di-*tert*-butylbenzo-1,2-quinone.[6] $Ru_3(CO)_{12}$ (100 mg, 1.5×10^{-4} mol) and 3,5-di-*tert*-butylbenzoquinone (300 mg, 1.4×10^{-3} mol) were dessolved in toluene (50 mL), and the reaction mixture was refluxed under N_2 for 6 h. After the solvent was removed under reduced pressure, the residue was dissolved in hexane, followed by loading on a silica gel column (3.5 × 15 cm). The second reddish purple band eluted with CH_2Cl_2 was collected and evaporated to dryness. The residue was dissolved in a small amount of EtOH followed by addition of water. The reddish purple compound thus precipitated was collected by filtration and dried under reduced pressure. Yield: 196 mg, 66%. IR (ν/cm^{-1}, KBr): 2000 (CO), 2058 (CO). UV–vis–NIR (λ_{max}/nm (ε/$M^{-1}\,cm^{-1}$), CH_2ClCH_2Cl): 297 (12200), 379 (3830), 544 (3500), 951 (5350). ESI-MS (m/z, CH_2Cl_2): 597 ([**5**]$^+$). Anal. Found: C, 60.05; H, 6.60%. Calcd for $C_{30}H_{40}O_6Ru$: C, 60.28; H, 6.75%.

[Ru(CO)$_2$(phsq)$_2$], [6]: To a toluene solution of 100 mg (0.15 mmol) of $Ru_3(CO)_{12}$ was added an excess of 9,10-phenanthraqui-

none (190 mg, 0.90 mmol); then the mixture was heated at reflux for 3 h under N_2. The solvent was removed on a rotary evaporator, and the residue was dissolved with CH_2Cl_2. The crude solution was purified by silica gel column chromatography using CH_2Cl_2 as an eluent. $[Ru(CO)_2(phsq)_2]$ appeared as a brown band. The volume of the solution was reduced until approximately 1 mL using a rotary evaporator. The brown crystals precipitated after addition of ether. The crystals were filtered off, washed with Et_2O, and dried in vacuo. Yield: 60 mg, 67%. IR (ν/cm^{-1}, KBr): 1975 (s, CO), 2049 (s, CO). UV–vis–NIR (λ_{max}/nm (ε/M^{-1} cm^{-1}), CH_2ClCH_2Cl): 321 (7990), 416 (1340), 915 (3730). FAB-MS (m/z): 584 ([**6**]$^+$). Anal. Found: C, 61.57; H, 2.95%. Calcd for $C_{30}H_{16}O_6Ru \cdot 0.25(CH_2Cl_2)$: C, 61.08; H, 2.80%.

Measurements. Electronic absorption spectra were recorded on a Shimadzu UV-3100PC spectrophotometer. Cyclic voltammograms of the complexes were obtained in dichloromethane or 1,2-dichloroethane containing 0.1 M of tetra-*n*-butylammonium perchlorate (TBAP) as a supporting electrolyte under N_2 by using an ALS/chi Electrochemical Analyzer Model 660. A glassy-carbon and a platinum wire were used as a working electrode and a counter electrode, respectively. Ag/Ag^+ reference electrode, purchased from BAS Inc, was separated from the working compartment by Vycor glass and composed of Ag wire and the acetonitrile solution of 0.01 M $AgNO_3$ and 0.1 M TBAP. IR spectra were obtained on a Shimadzu FTIR-8100 spectrometer. UV–vis–NIR spectra under electrolysis conditions were obtained by using a thin-layer electrode cell with a platinum minigrid working electrode sandwiched between two glass sides of an optical cell (path length 0.5 mm), where an Ag/Ag^+ reference electrode was separated from the working compartment by Vycor glass. Hokuto Denko HA-151 potentiostat/function generator was used. IR measurements under the electrolysis conditions were performed with a thin layer electrode cell with a platinum mesh grid working electrode sandwiched between two KBr crystals (the path length; 0.5 mm). ESR spectra were measured with a JEOL X-band spectrometer (JES-RE1XE). The g values were calibrated precisely with a Mn^{2+} marker, which was used as a reference. Electro-spray mass spectra were obtained on a Shimadzu LC-MS 2100 mass spectrometer. FAB mass spectra were obtained on a JEOL JMS-GC mate II GCMS system with a FAB-MS unit.

Crystallography. Single crystals of [**1**]$(ClO_4)\cdot 2(C_7H_8)$ were obtained by the exchange of the counter anion from PF_6^- to ClO_4^- followed by slow diffusion of toluene into an acetonitrile solution of [**1**](ClO_4). The single crystals of [**6**] were obtained from a CH_2Cl_2 solution. A summary of the crystal structure refinements of the compounds [**1**](ClO_4) and [**6**] were given in Table 1. Data were collected on a Rigaku/MSC Mercury CCD diffractometer using graphite monochromated Mo Kα radiation ($\lambda = 0.71070$ Å) at 173 K, and processed using Crystal Clear.[13] The structure of [**1**]$(ClO_4)\cdot 2(C_7H_8)$ was solved by a heavy-atom Patterson method (PATTY)[14] and expanded using Fourier Techniques (DIRDIF94).[15] The structure was refined by full-matrix least-square refinement on F^2. All non-hydrogen atoms were refined with anisotropic displacement parameters with the exception of those of crystal solvents. All hydrogen atoms were located on the calculated positions and were not refined. The structure of [**6**] was solved by a direct method (SIR92)[16] and refined by full-matrix least-square refinement on F^2. All non-hydrogen atoms were refined with anisotropic displacement parameters. All hydrogen atoms were located on the calculated positions and were not refined. All calculations were performed using the teXsan crystallographic software package.[17] Crystallographic data for the structural analysis of [**1**]$(ClO_4)\cdot 2(C_7H_8)$ and [**6**] have been deposited with the Cambridge Crystallographic Data Centre, CCDC No. 208579 and No. 208580, respectively (www:http://ccdc.cam.ac.uk).

References

1 a) M. D. Ward and J. A. McCleverty, *J. Chem. Soc., Dalton Trans.*, **2002**, 275. b) C. G. Pierpont, *Coord. Chem. Rev.*, **216**, 99 (2001). c) S. I. Gorelsky, E. S. Dodsworth, A. B. P. Lever, and A. A. Vlcek, *Coord. Chem. Rev.*, **174**, 469 (1998). d) C. G. Pierpont and C. W. Lange, *Prog. Inorg. Chem.*, **41**, 331 (1994). e) A. B. P. Lever, H. Masui, R. A. Metcalfe, D. J. Stufkens, E. S. Dodsworth, and P. R. Auburn, *Coord. Chem. Rev.*, **125**, 317 (1993).

2 a) M. Ebadi and A. B. P. Lever, *Inorg. Chem.*, **38**, 467 (1999). b) K. Yang, J. A. Martin, S. G. Bott, and M. G. Richmond, *Inorg. Chim. Acta*, **254**, 19 (1997). c) W. Paw, J. B. Keister, C. H. Lake, and M. R. Churchill, *Organometallics*, **14**, 767 (1995). d) R. S. da Silva, E. Tfouni, and A. B. P. Lever, *Inorg. Chim. Acta*, **235**, 427 (1995). e) N. Bag, G. K. Lahiri, P. Basu, and A. Chakravorty, *J. Chem. Soc., Dalton Trans.*, **1992**, 113. f) N. Bag, A. Pramanik, G. K. Lahiri, and A. Chakravorty, *Inorg. Chem.*, **31**, 40 (1992). g) S. Bhattacharya and C. G. Pierpont, *Inorg. Chem.*, **31**, 35 (1992). h) S. Bhattacharya and C. G. Pierpont, *Inorg. Chem.*, **30**, 1511 (1991). i) P. R. Auburn, E. S. Dodsworth, M. Haga, W. Liu, W. A. Nevin, and A. B. P. Lever, *Inorg. Chem.*, **30**, 3502 (1991). j) S. R. Boone and C. G. Pierpont, *Polyhedron*, **9**, 2267 (1990). k) M. Haga, K. Isobe, S. R. Boone, and C. G. Pierpont, *Inorg. Chem.*, **29**, 3795 (1990). l) D. J. Stufkens, Th. L. Snoeck, and A. B. P. Lever, *Inorg. Chem.*, **27**, 953 (1988). m) A. B. P. Lever, P. R. Auburn, E. S. Dodsworth, M. Haga, W. Liu, M. Melnik, and W. A. Nevin, *J. Am. Chem. Soc.*, **110**, 8076 (1988). n) S. R. Boone and C. G. Pierpont, *Inorg. Chem.*, **26**, 1769 (1987). o) M. Haga, E. S. Dodsworth, and A. B. P. Lever, *Inorg. Chem.*, **25**, 447 (1986). p) M. Haga, E. S. Dodsworth, A. B. P. Lever, S. R. Boone, and C. G. Pierpont, *J. Am. Chem. Soc.*, **108**, 7413 (1986). q) S. D. Pell, R. B. Salmonsen, A. Abelleira, and M. J. Clarke, *Inorg. Chem.*, **23**, 385 (1984).

3 M. Kurihara, S. Daniele, K. Tsuge, H. Sugimoto, and K. Tanaka, *Bull. Chem. Soc. Jpn.*, **71**, 867 (1998).

4 a) K. Tsuge and K. Tanaka, *Chem. Lett.*, **1998**, 1069. b) K. Tsuge, M. Kurihara, and K. Tanaka, *Bull. Chem. Soc. Jpn.*, **73**, 607 (2000). c) K. Kobayashi, H. Ohtsu, T. Wada, and K. Tanaka, *Chem. Lett.*, **2002**, 868. d) K. Kobayashi, H. Ohtsu, T. Wada, T. Kato, and K. Tanaka, *J. Am. Chem. Soc.*, **125**, 6729 (2003).

5 H. Sugimoto and K. Tanaka, *J. Organomet. Chem.*, **622**, 280 (2001).

6 S. Bhattacharya and C. G. Pierpont, *Inorg. Chem.*, **33**, 6038 (1994).

7 J. V. Caspar, B. P. Sullivan, and T. J. Meyer, *Organometallics*, **2**, 551 (1983).

8 H. Ishida, K. Tanaka, M. Morimoto, and T. Tanaka, *Organometallics*, **5**, 724 (1986).

9 H. Nakajima, Y. Kushi, H. Nagao, and K. Tanaka, *Organometallics*, **14**, 5093 (1995).

10 R. A. T. M. Abbenhuis, I. der Rio, M. M. Bergshoef, J. Boersma, N. Veldman, A. L. Spek, and G. van Koten, *Inorg. Chem.*, **37**, 1749 (1998).

11 S. Bhattacharya, S. R. Boone, G. A. Fox, and C. G. Pierpont, *J. Am. Chem. Soc.*, **112**, 1088 (1990).

12 B. M. Holligan, J. C. Jeffery, M. K. Norgett, E. Schatz, and M. D. Ward, *J. Chem. Soc., Dalton Trans.*, **1992**, 3345.

13 Crystal Clear Software Package, Riganku and Molecular

Structure Corp. (1999).

14 PATTY: P. T. Beurskens, G. Admiraal, G. Beukens, W. P. Bosman, R. de Gelder, R. Israel, and J. M. M. Smith, "The DIRDIF-94 program system: Technical Report of the Crystallography Laboratory," University of Nijmengen, the Netherlands (1994).

15 DIRDIF94: P. T. Beurskens, G. Admiraal, G. Beukens, W. P. Bosman, R. de Gelder, R. Israel, and J. M. M. Smith, "The DIRDIF-94 program system: Technical Report of the Crystallography Laboratory," University of Nijmengen, the Netherlands (1994).

16 SIR92: A. Altomare, M. C. Burla, M. Camalli, M. Cascarano, C. Giacovazzo, A. Guagliardi, and G. Polidori, *J. Appl. Crystallogr.*, **27**, 435 (1994).

17 teXsan: Cryatal Structure Analysis Package, Molecular Structure Corporation (1992).

18 F. A. Cotton and C. S. Kraihanzel, *J. Am. Chem. Soc.*, **84**, 4432 (1962).